JOURNAL OF SPACECRAFT AND ROCKETS
Vol. 36, No. 2, March–April 1999

Aeroheating Predictions for X-34 Using an Inviscid Boundary-Layer Method

Christopher J. Riley* and William L. Kleb†
NASA Langley Research Center, Hampton, Virginia 23681
and
Steven J. Alter‡
Lockheed Engineering and Sciences Company, Hampton, Virginia 23681

Radiative equilibrium surface temperatures and surface heating rates from a combined inviscid boundary-layer method are presented for the X-34 reusable launch vehicle for several points along the hypersonic descent portion of its trajectory. Inviscid, perfect-gas solutions are generated with the LAURA and the DPLUR codes. Surface temperatures and heating rates are then computed using the LATCH engineering code employing both laminar and turbulent flow models. The combined inviscid boundary-layer method provides accurate predictions of surface temperatures over most of the vehicle and requires much less computational effort than a Navier–Stokes code. This engineering method enables the generation of a more thorough aerothermal database, which is necessary to design the thermal protection system and specify the vehicle's flight limits.

Nomenclature

M = Mach number
q_{stg} = stagnation heating rate, Btu/ft^2-s
q_w = wall heating rate, Btu/ft^2-s
R_n = nose radius, ft
T_w = wall temperature, °F
t = time along trajectory, s
x = axial coordinate, in.
z = lateral coordinate, in.
α = angle of attack, deg
δ_{el} = elevon deflection, deg

Introduction

THE X-34 (Refs. 1–6) is a reusable, suborbital test vehicle developed by Orbital Sciences Corporation (OSC) as part of NASA's reusable launch vehicle (RLV) technology program.[7] Originally proposed as a partially reusable, two-stage vehicle designed to deliver 1500 lb to low Earth orbit, the X-34's current purpose is to provide a test bed for RLV technologies and to demonstrate RLV operations. These technologies include autonomous landing systems, low-cost avionics, advanced thermal protection systems (TPS), and composite airframe and propellant tanks. Relatively small in size, the X-34 is 58 ft long with a wing span of 28 ft and a gross weight of approximately 45,000 lb. One of the program's goals is to develop a vehicle capable of achieving Mach 8 flight and an altitude of 250,000 ft. Part of NASA Langley Research Center's role in the X-34 program is to assist OSC by performing both computational fluid dynamic (CFD) analysis on the vehicle as well as aerodynamic and aeroheating wind-tunnel testing. One of Langley's tasks is to provide OSC with CFD predictions of entry heating rates to be used for the TPS design.

The design of a vehicle's TPS involves two areas. First, the maximum surface temperature along a trajectory defines which materials may be used for the TPS over different regions of the vehicle. Conversely, once the TPS materials have been chosen, flight limits are required to ensure the temperature limits of the materials are not violated for off-nominal trajectories. CFD assists in this area with solutions at or near the peak heating point (as defined by a stagnation heating rate) of a trajectory. Second, the total heat load over the flight trajectory defines the thickness of the TPS materials. Full CFD is not appropriate. Long computer run times for individual Navier–Stokes (N–S) solutions prohibit running the many solutions required to define the heating along a trajectory. Instead, engineering codes such as MINIVER[8] are typically used to provide the complete time histories of surface heating used to compute total heat load.

Another approach to defining the surface heating along a trajectory is to use a combined inviscid boundary-layer method. Inviscid CFD solutions coupled with a heating technique are less costly than N–S solutions; therefore, more points on a trajectory can be computed using the same computer resources. Also, engineering boundary-layer methods such as the LATCH code[9] provide reasonably accurate heating rates over much of the vehicle (e.g., stagnation region, wind side, regions without flow separation) and run in minutes on desktop workstations. However, care must be exercised at high-altitude, low-Reynolds-number conditions where the shock layer cannot be divided into separate inviscid and boundary-layer regions due to viscous interactions. At these conditions an inviscid boundary-layer approach is inappropriate, and methods that treat the entire shock layer as viscous, such as viscous-shock layer,[10] parabolized N–S,[11] or N–S solvers, are necessary. Inviscid boundary-layer methods are not meant to replace but complement benchmark CFD solutions in the area of TPS design. Although it may still be prohibitive to cover a trajectory in detail using this approach, heating rates computed at selected points on the trajectory can be used to calibrate the temperature time histories from an engineering method.[12]

This paper details the use of an inviscid boundary-layer method to compute the surface heating rates over the X-34 at several points along a representative trajectory supplied by OSC. Inviscid, perfect-gas solutions are generated with the LAURA and the DPLUR codes. LATCH is used to compute the surface heating rates and radiative equilibrium temperatures. Comparisons of the surface heating rates and temperatures are made with viscous, thin-layer N–S solutions from LAURA.[13] Comparisons with experimental aeroheating data are found in Ref. 14. Maximum wind-side, lee-side, and wing leading-edge temperatures are estimated as well. This work is part of a collective effort at NASA Langley Research Center to provide OSC with the aerothermal information necessary to design the TPS for the

Received Feb. 25, 1998; revision received July 24, 1998; accepted for publication Aug. 1, 1998.

*Research Engineer, Aerothermodynamics Branch, Aero- and Gas-Dynamics Division. Senior Member AIAA.
†Research Engineer, Aerothermodynamics Branch, Aero- and Gas-Dynamics Division.
‡Senior Aeronautical Engineer. Senior Member AIAA.

X-34 vehicle. Additional data delivered to OSC by NASA Langley Research Center include benchmark CFD solutions,[13] experimental aeroheating,[14] and time histories of surface temperature.[12]

Geometry

The full X-34 vehicle configuration (version X0001215) is shown in Fig. 1a, and the geometry used for the inviscid solutions is shown in Fig. 1b. Gaps in the elevons and between different TPS materials are not modeled. Because LATCH requires a single block topology, the area aft of the wing trailing edge (including the vertical tail and body flap) is not included in the inviscid geometry.

Trajectory

The X1004601 no-bounce trajectory that is analyzed is shown in Figs. 2–5. This no-bounce trajectory is designed to eliminate the possibility of bouncing off of the atmosphere after re-entry and is used as the reference trajectory for maximum wind-side and lee-side heating. The angle of attack varies from 25 to 8 deg during the hypersonic descent portion of the trajectory. At the request of OSC, the following inviscid boundary-layer cases (2 ascent, 4 descent) are computed and are listed in Table 1: For this paper the cases presented in detail are the $M = 6.32, \alpha = 23$ deg case ($t = 330$ s) and the $M = 6$, $\alpha = 15.22$ deg case ($t = 340$ s) because N–S solutions exist for these. Nonetheless, all inviscid boundary-layer solutions

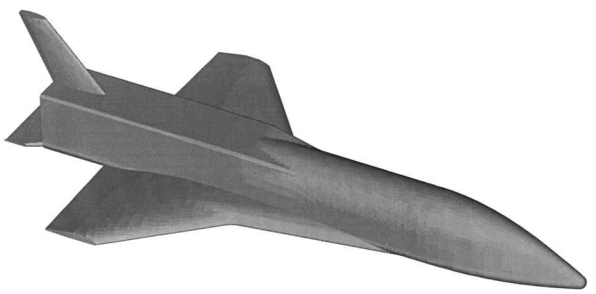

a) Full configuration used for viscous solutions

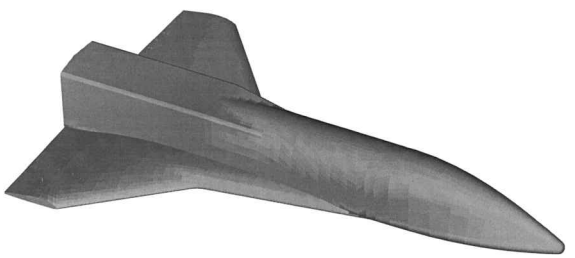

b) Partial configuration used for inviscid solutions

Fig. 1 X-34 configurations.

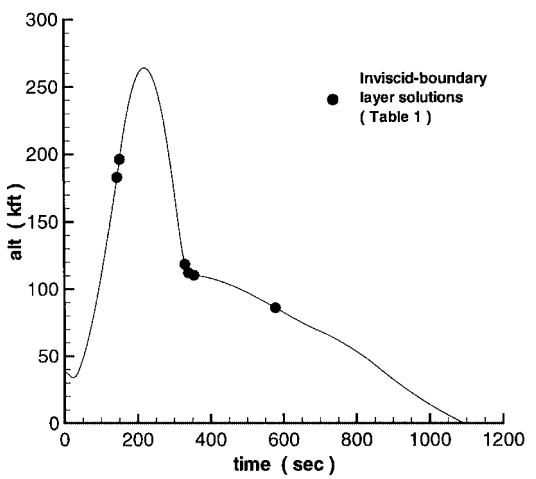

Fig. 2 X1004601 trajectory altitude.

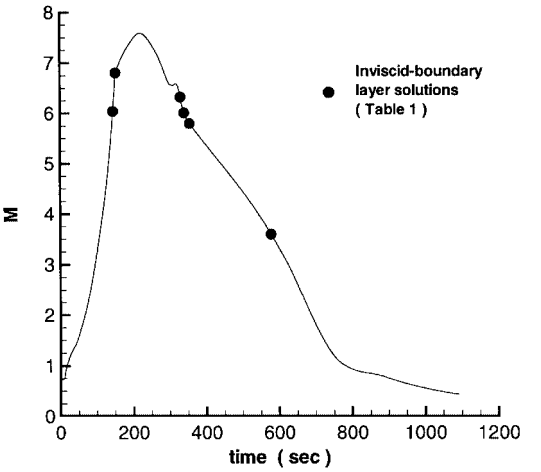

Fig. 3 X1004601 trajectory Mach number.

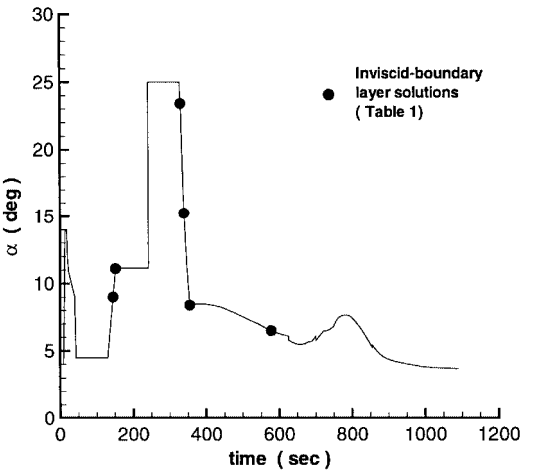

Fig. 4 X1004601 trajectory angle of attack.

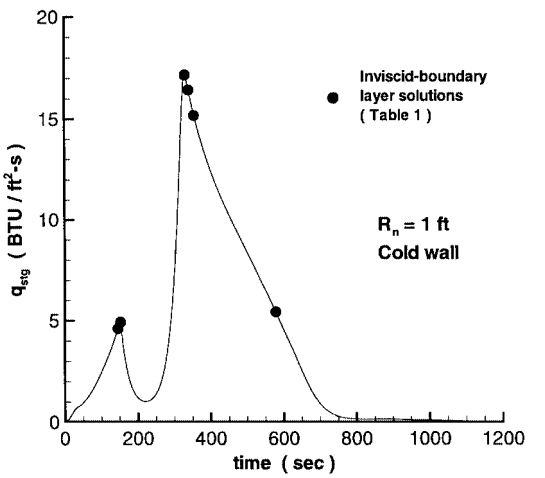

Fig. 5 X1004601 trajectory stagnation point heating.

are used to compute the time histories of surface temperature used for the TPS design as detailed in Ref. 12.

Computational Mesh

The inviscid volume grid is obtained by truncating a viscous volume grid for the X-34 at the wing trailing edge. Because the viscous grid contains many grid points to resolve gradients, the inviscid grid is thinned, and the points are redistributed to reduce unnecessary clustering. The resulting inviscid volume grid is $120 \times 152 \times 32$ cells. The corresponding viscous volume grid contains 64 cells between the body and grid outer boundary. Grid resolution studies in

Table 1 Inviscid boundary-layer solutions[a]

Time, s	Altitude, kft	Mach no.	α, deg	δ_{el}, deg	Inviscid code used	N–S solution available?	Note
145	183	6	9	0	LAURA	No	Mach 6 ascent
152	196	6.83	11	0	LAURA	No	Maximum heating on ascent
*330	118	6.32	23	0	DPLUR	Yes	Maximum heating
——	——	——	——	+10	LAURA	Yes	——
*340	112	6	15.22	0	DPLUR	Yes	Wind-tunnel comparison
355	110	5.8	8	−10	LAURA	No	Minimum α, maximum heating
578	86	3.6	6.46	−10	LAURA	No	Re-entry maximum q, maximum heating

[a]*, Presented in detail.

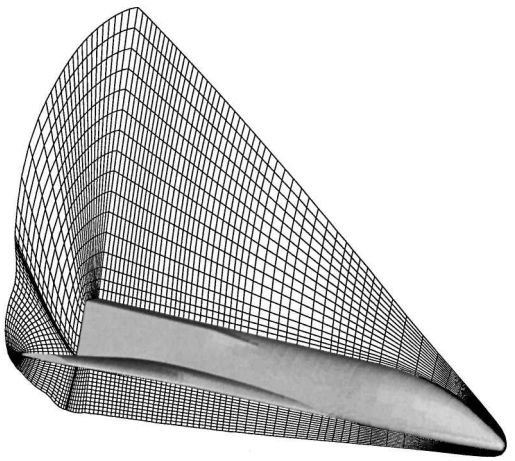

Fig. 6 Inviscid flowfield grid (coarsened).

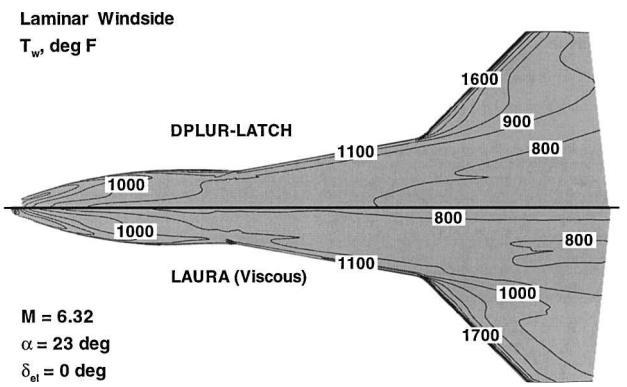

Fig. 7 Laminar wind-side temperatures at t = 330 s.

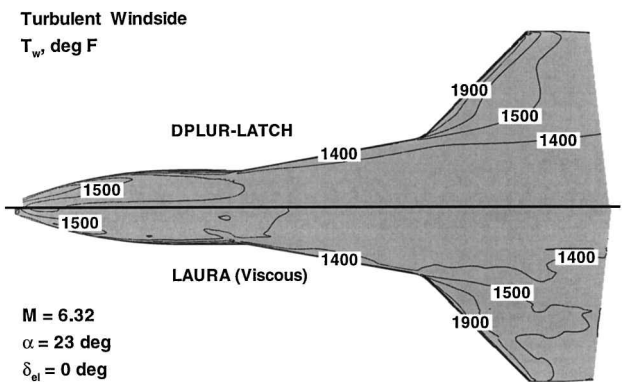

Fig. 8 Turbulent wind-side temperatures at t = 330 s.

Ref. 15 indicate 32 cells are sufficient for inviscid calculations. Although DPLUR used this grid size for both of its solutions, LAURA's multiblock capabilities allowed a coarser grid in the circumferential direction to be used in the nose region for its computations. This coarsening of the grid speeds convergence of the solution in the stagnation region. Details of the grid generation process for the X-34 vehicle are given in Ref. 16. A sample, coarsened, flowfield grid is shown in Fig. 6.

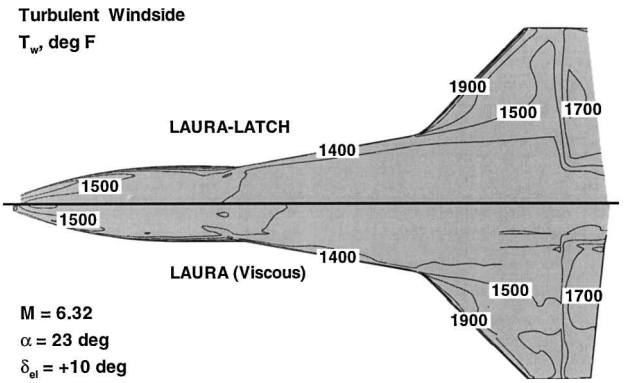

Fig. 9 Turbulent wind-side temperatures at t = 330 s (with elevons deflected).

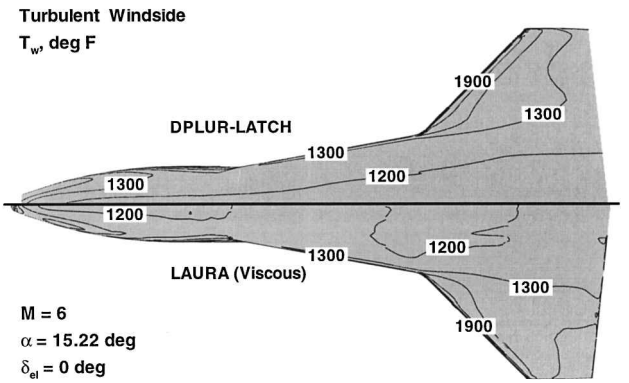

Fig. 10 Turbulent wind-side temperatures at t = 340 s.

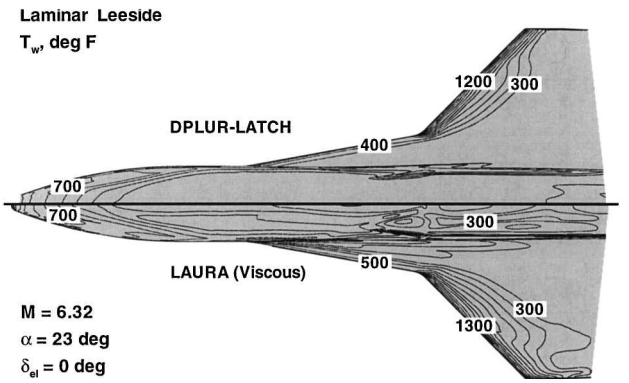

Fig. 11 Laminar lee-side temperatures at t = 330 s.

Flowfield Codes

Inviscid solutions for the cases listed in Table 1 are generated with the CFD codes LAURA and DPLUR. To provide surface heating information to OSC in a timely fashion, two codes are used instead of one. Each code is tuned for a different computer architecture: LAURA for multitasking vector computers and DPLUR for massively parallel machines. Solutions for the database can be run concurrently on different systems to save time. The inviscid flowfields serve as inputs to the LATCH engineering code, which computes surface streamlines and both laminar and turbulent heating

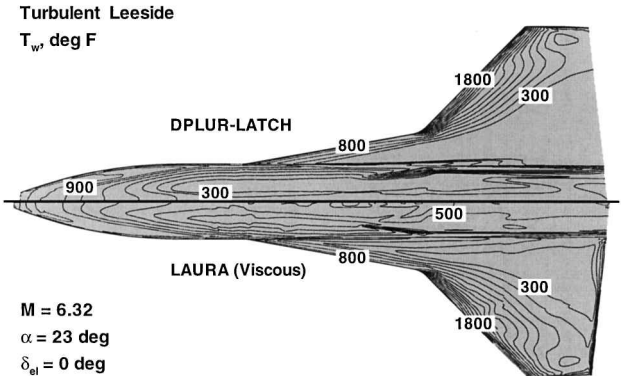

Fig. 12 Turbulent lee-side temperatures at t = 330 s.

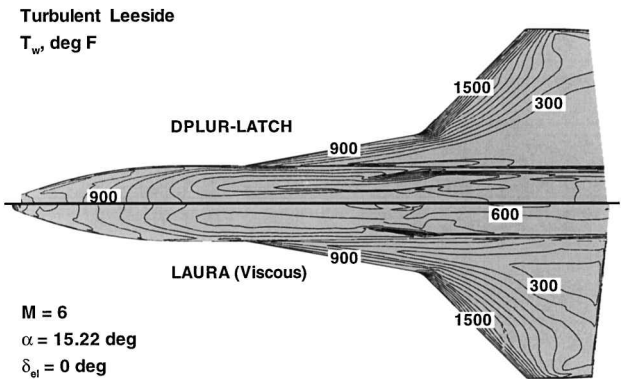

Fig. 13 Turbulent lee-side temperatures at t = 340 s.

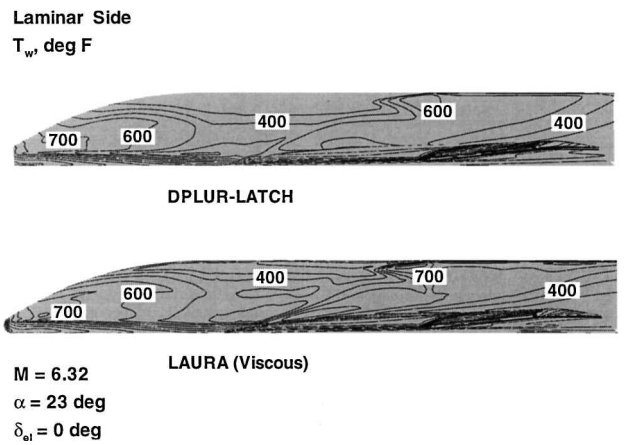

Fig. 14 Laminar side temperatures at t = 330 s.

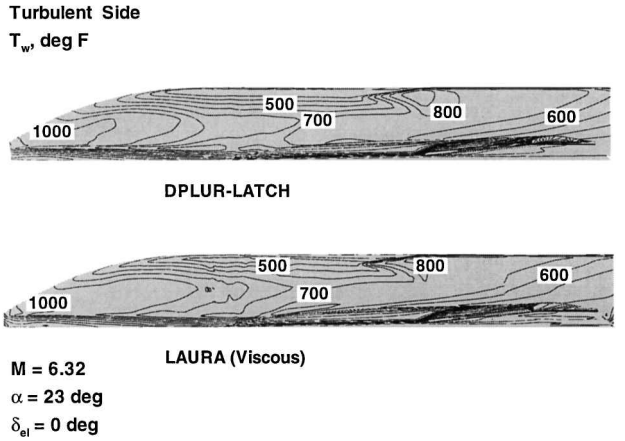

Fig. 15 Turbulent side temperatures at t = 330 s.

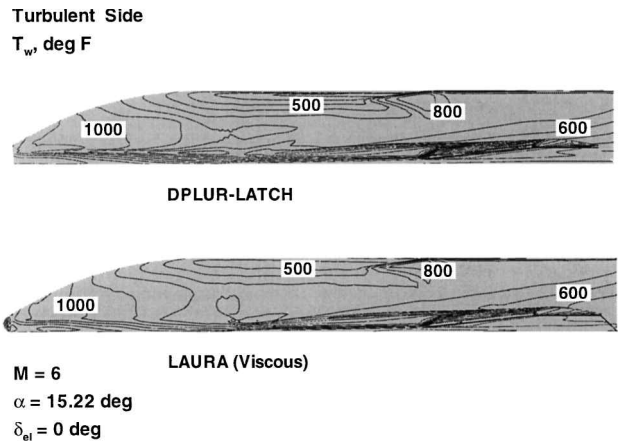

Fig. 16 Turbulent side temperatures at t = 340 s.

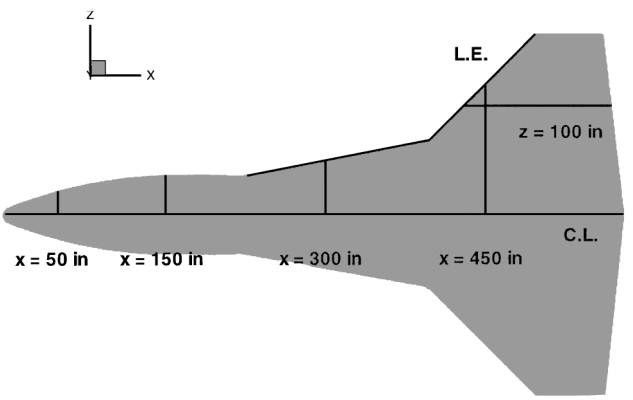

Fig. 17 Cut plane locations.

rates. Brief descriptions of the three methods are in the following paragaraphs.

LAURA

LAURA is a finite volume, shock-capturing algorithm for the steady-state solution of inviscid or viscous, hypersonic flows on rectangularly ordered, structured grids. LAURA has been used extensively to provide aerothermodynamic characteristics for a number of aerospace vehicles [e.g., Aeroassist Flight Experiment,[17] HL-20 (Ref. 18), Shuttle Orbiter,[19] Mars Pathfinder,[20] Single-Stage-to-Orbit Access to Space[21]] and is currently being used in the design and evaluation of the X-33 RLV (Ref. 22). The upwind-biased inviscid flux is constructed using Roe's flux-difference splitting[23] and Harten's entropy fix[24] with second-order corrections based on Yee's symmetric total-variation-diminishing scheme.[25] A point-implicit strategy is used that treats the variables at the cell center of interest implicitly at the advanced iteration level and uses the latest available data from neighboring cells. This strategy results in an efficient, parallel implementation on multitasking vector computers.[26] Gas chemistry options include perfect gas, equilibrium air, and air in chemical and thermal nonequilibrium. The algebraic turbulence models of Cebici[27] and Baldwin–Lomax[28] are also available. More details of the algorithm can be found in Refs. 26, 29, and 30.

DPLUR

The DPLUR method[31,32] is based on the lower–upper symmetric Gauss–Seidel method of Yoon and Jameson[33] but has been modified for data-parallel computing. The Gauss–Seidel sweeps of the original method of Yoon and Jameson are replaced with a series of point Jacobi-like subiterations. This modification removes all data dependencies and yields a method that is almost perfectly parallel. Like LAURA, it is a finite volume, shock-capturing algorithm for the steady-state solution of both inviscid and viscous flowfields on structured grids. Presently, there are options for

perfect gas, equilibrium air, and five-species nonequilibrium gas chemistry.

LATCH

The engineering code LATCH[9] computes surface heating rates on three-dimensional vehicles at angle of attack. The method is based on the axisymmetric analog for three-dimensional boundary layers and uses a generalized body-fitted coordinate system. Boundary-layer edge conditions and the surface velocities used to determine inviscid streamline direction are obtained from an inviscid flowfield solution. In this paper inviscid solutions are supplied by both LAURA and DPLUR. Instead of solving the boundary-layer equations along streamlines, an approximate heating method developed by Zoby and Simmonds[34] that is valid for both laminar and turbulent heating is used. This method has been shown to produce accurate results for both wind-tunnel and flight conditions[34–36] with only a fraction of the computational effort required by the full boundary-layer equations.

Computational Resources

The primary advantage to using an inviscid boundary-layer method over an N–S code is the reduction in time needed to generate a solution. For the inviscid cases listed in Table 1, DPLUR requires 100 node h per solution on an IBM SP-2, and LAURA requires about 25 h per solution on a Cray Y-MP. LATCH boundary-layer solutions containing surface temperatures and heating rates are then obtained in about 5 min each on an SGI R10000 workstation. Conversely, the viscous LAURA solutions require approximately 300 h each on a Cray C-90 to reach convergence. Although the inviscid boundary-layer approach still uses a considerable amount of computer time and resources compared to pure engineering methods, it offers a significant savings over viscous N–S CFD codes.

Results

Surface temperature contours and heating rates are examined for the X-34 at $M = 6.32$, $\alpha = 23$ deg ($t = 330$ s) and $M = 6$, $\alpha = 15.22$ deg ($t = 340$ s). Results from a combined inviscid boundary-layer method (LAURA–LATCH and DPLUR–LATCH) are compared with viscous solutions from LAURA to assess the accuracy of the inviscid boundary-layer approach. Additional comparisons with experimental aeroheating data are given in Ref. 14. Both laminar and turbulent solutions are computed although OSC only requested turbulent heating data. All solutions assume a perfect gas and compute radiative equilibrium wall temperatures based on an emissivity of 0.8. The turbulent, viscous solutions from LAURA are computed using the Baldwin–Lomax algebraic turbulence model. Details of the LAURA viscous solutions are found in Ref. 13.

Wind-side temperature contours are shown in Figs. 7–10 for the two flight conditions. Contour levels are plotted in 100°F increments over a range of temperatures from 300 to 2000°F. The upper half of each figure depicts the inviscid boundary-layer results (either LAURA–LATCH or DPLUR–LATCH), and the lower half shows the surface temperatures from a LAURA viscous solution. To help correlate the predicted surface temperatures with TPS materials, Table 2 lists the multiuse capability of the TPS blankets used over much of the vehicle. In Fig. 7 the laminar temperatures from

Table 2 Multiuse temperature limits of TPS blankets

Material	Maximum temperature, °F
High heat blanket	2000
Low heat blanket	1500
FRSI	700

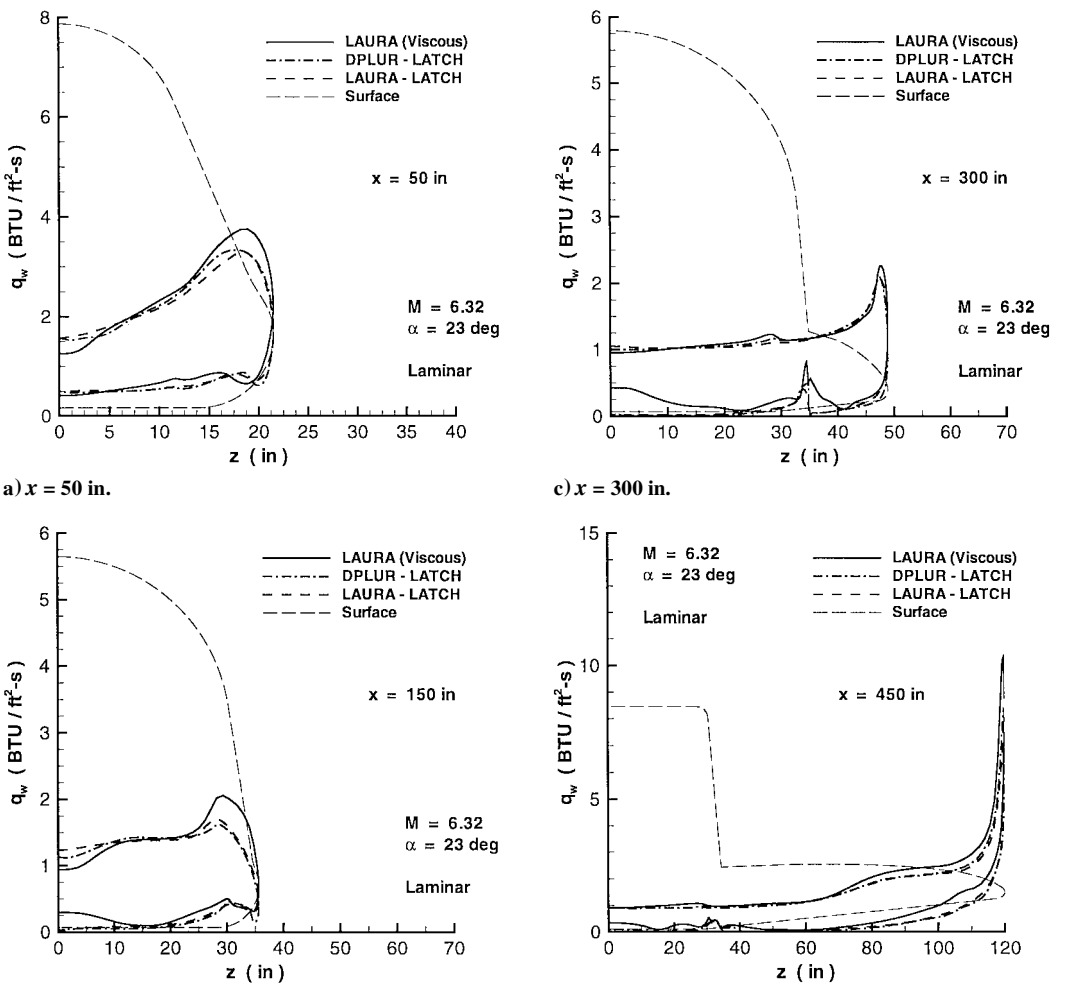

a) $x = 50$ in. c) $x = 300$ in.

b) $x = 150$ in. d) $x = 450$ in.

Fig. 18 Lateral laminar heating distributions at $t = 330$ s.

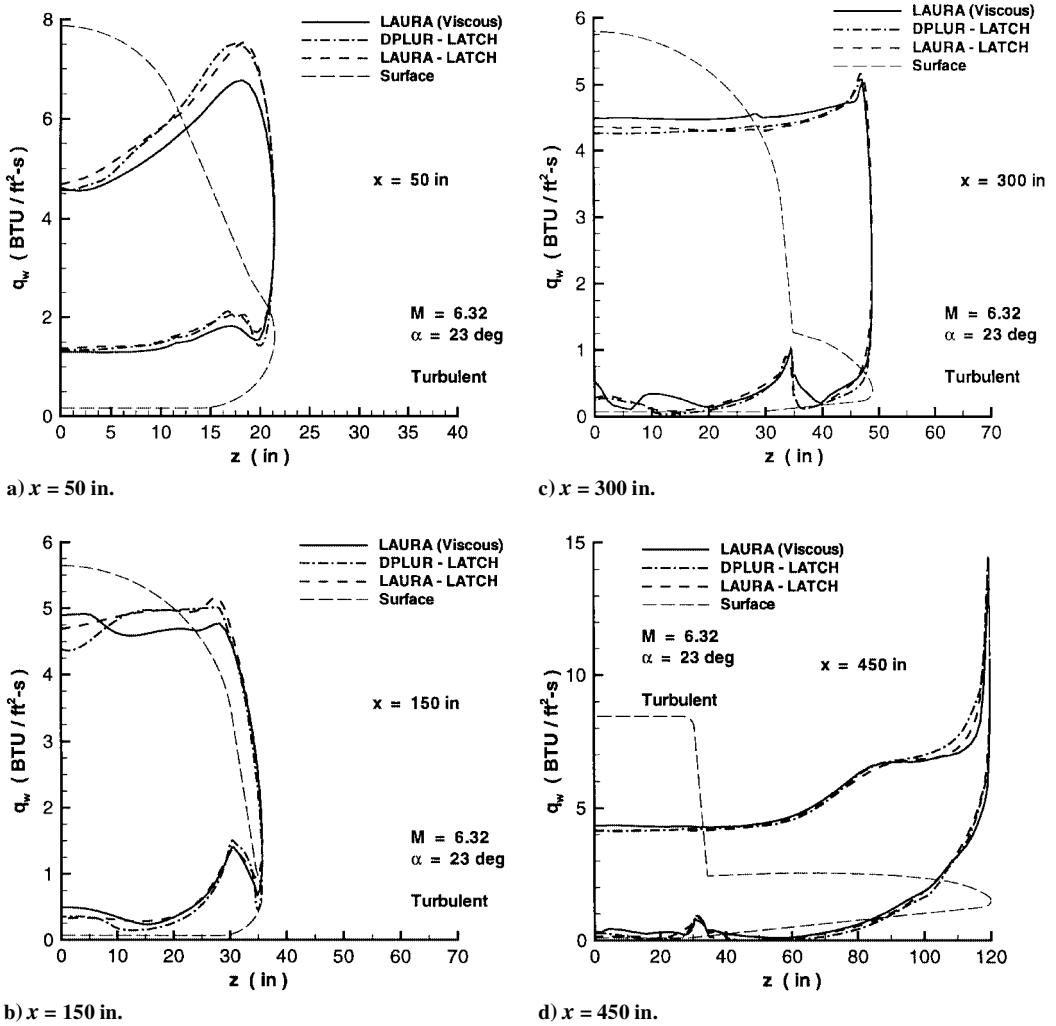

Fig. 19 Lateral turbulent heating distributions at t = 330 s.

DPLUR–LATCH agree quite well (i.e., within 100°F) with the temperatures from LAURA over much of the lower surface. Both solutions predict temperatures of 800°F near the centerline, 1100°F near the outer edge of the strake, and 900–1000°F near the middle of the wing. This region of higher temperatures extending across the wing from the leading to the trailing edge is caused by the wing bow-shock interaction and is predicted by both methods. However, the magnitude of the temperatures appears to be slightly lower for DPLUR–LATCH. Similar comparisons are seen for the turbulent results shown in Figs. 8–10, albeit the overall temperature levels are 300–600°F higher than the laminar temperatures. The higher temperatures force the use of the high heat blanket (HHB) over much of the windward surface. Figure 9 shows the temperature contours for the X-34 with +10-deg deflected elevons. Both LAURA–LATCH and LAURA show a pocket of higher temperatures (≈1700°F) on the elevon surface. In addition, Figs. 8 and 9 offer a comparison between DPLUR–LATCH and LAURA–LATCH solutions at the same conditions (except for the elevon deflection). The temperature contours for the two solutions are similar over much of the lower surface except near the forward portion of the vehicle where DPLUR–LATCH predicts a lower temperature away from the centerline. As previously stated, a coarser grid was used for the inviscid LAURA solution in the circumferential direction in this region, which may account for some of the differences. Figure 10 shows the wind-side temperature contours for $t = 340$ s. As expected, the lower angle of attack ($\alpha = 15.22$ deg) results in generally lower temperatures on the wind side of the vehicle. For example, the radiative equilibrium temperatures over most of the wing are around 200°F lower than for the $t = 330$ s case.

Lee-side temperature contours are shown in Figs. 11–13. Temperature contours for the turbulent, deflected elevon case at $t = 330$ s are not presented because the lee-side temperatures on the elevon are very low (<300°F). Somewhat unexpectedly for an inviscid boundary-layer method, the lee-side temperature contours from DPLUR–LATCH agree quite well with the viscous LAURA solution at these conditions. The same general patterns in temperature are seen near the forward portion of the vehicle as well as on the wing. These lee-side predictions impact the TPS design because the temperature levels vary around the limit of the flexible reusable surface insulation (FRSI) blankets (700°F).

Temperature contours on the side of the vehicle are shown in Figs. 14–16. Again the contour patterns from DPLUR–LATCH and the viscous LAURA solutions are very similar. Therefore, as seen in Figs. 7–16, the inviscid boundary-layer technique predicts radiative equilibrium wall temperatures that compare favorably with temperatures from an N–S solver.

To illustrate the differences between the inviscid boundary layer and N–S solutions more clearly, surface heating rates are examined along several cut planes including centerline, wing leading edge, and cross-sectional cuts. Surface heating rates are more sensitive than radiative equilibrium wall temperatures ($q_w \sim T_w^4$) and should provide more insight into the comparison between the methods. The locations of cut planes are shown in Fig. 17.

Lateral surface heating distributions are given in Figs. 18–20 at four axial stations. The laminar heating rates in Fig. 18 are examined first because there is no influence of different turbulence models. The laminar cuts in Fig. 18 show, in general, an overall good agreement between the DPLUR–LATCH, LAURA–LATCH,

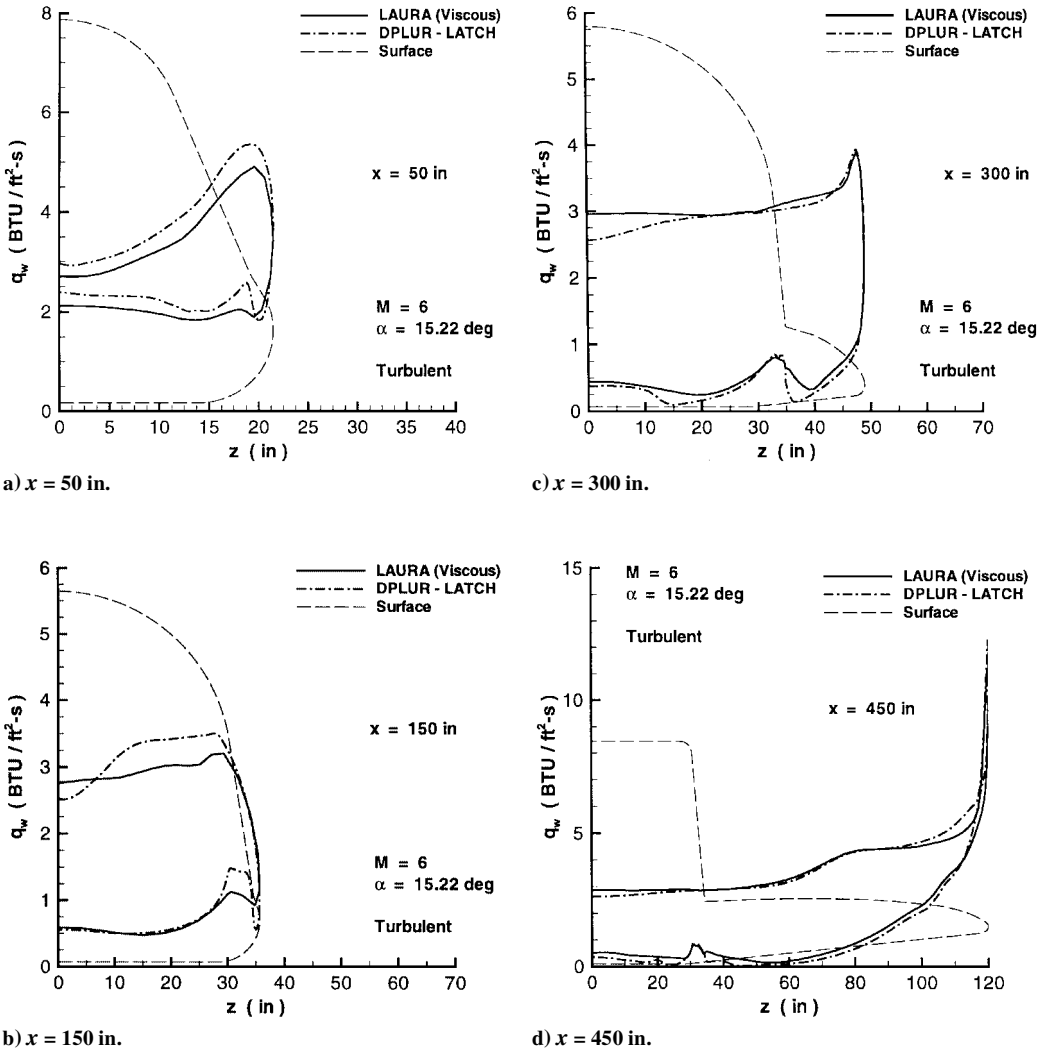

Fig. 20 Lateral turbulent heating distributions at t = 330 s.

and the viscous LAURA solutions. However, the LATCH results tend to underestimate the maximum heating rates from LAURA by approximately 15–20% at each axial station. Because LATCH computes heating rates along inviscid surface streamlines, it has difficulties in regions of high curvature such as near the wing leading edge. The surface streamlines cannot account for the large three-dimensional effects that are present. In particular, laminar heating rates from LATCH in high-curvature regions tend to be lower than those predicted by N-S solvers.[9] This may help explain the heating rate comparisons in Figs. 18c and 18d and to a lesser degree in Figs. 18a and 18b where the streamlines wrap from the lower surface around to the side of the vehicle.

Differences in the heating pattern near the windward centerline are noted in Figs. 18a and 18b between LATCH and LAURA. The heating decreases as the centerline is approached. A possible explanation is suggested by the DPLUR–LATCH and LAURA–LATCH results in Fig. 18b. LAURA–LATCH, which uses a coarser circumferential grid in this region, does not predict the dip in heating as well as DPLUR–LATCH, which uses the full grid. The streamline directions on the flat lower surface of the vehicle are sensitive to the grid resolution. Also seen in Figs. 18b and 18c is the increased heating predicted by LAURA near the leeward centerline. Cross-flow separation is present around $x = 150$ in. on the lee side of the vehicle,[13] and this is reflected in the higher heating rates. Being an engineering code that uses an inviscid solution, LATCH cannot predict this.

The turbulent heating rates in Figs. 19 and 20 are examined next. In general, good agreement between LATCH and LAURA is seen in the cross-sectional cuts, especially on the wing at $x = 300$ and 450 in. However, unlike the laminar results, the turbulent peak heating rates from LATCH tend to be higher than those from LAURA. This fact can be attributed to the inherent differences between the engineering turbulent boundary-layer equations in LATCH and the algebraic model employed by LAURA. For the turbulent cases the heating patterns near the windward centerline in Figs. 19b and 20b differ between LATCH and LAURA. Vortices on the wind side of the vehicle in the boundary layer that might explain these differences have been observed in the flowfields predicted by LAURA.[13] However, to keep the comparisons in perspective, differences of 15–20% in heating rates with corresponding differences of 4–5% in temperature are adequate for design work.

Windward centerline distributions for the two cases ($t = 330$ and 340 s) are presented in Fig. 21. The turbulent heating rates from LATCH (with both LAURA and DPLUR) are approximately 15% lower than the heating rates from LAURA for most of the vehicle ($x > 100$ in.) for both cases. The laminar heating rates in Fig. 21a from LATCH are 25% higher than the LAURA results for the forward half of the vehicle ($x < 300$ in.) The agreement is much better downstream. The heating rates from DPLUR–LATCH are closer to the LAURA heating rates because of the denser circumferential grid resolution used by DPLUR.

Wing leading-edge heating distributions are presented in Figs. 22–24. The leading edge is defined as the outermost point of the wing ($z = z_{max}$; see Fig. 17) and does not necessarily represent the highest heating rates or temperatures on the wing. In Fig. 22 the laminar heating rates from LAURA are approximately 15% higher than the inviscid boundary-layer (DPLUR–LATCH and LAURA–LATCH) solutions along the wing leading edge. This corresponds

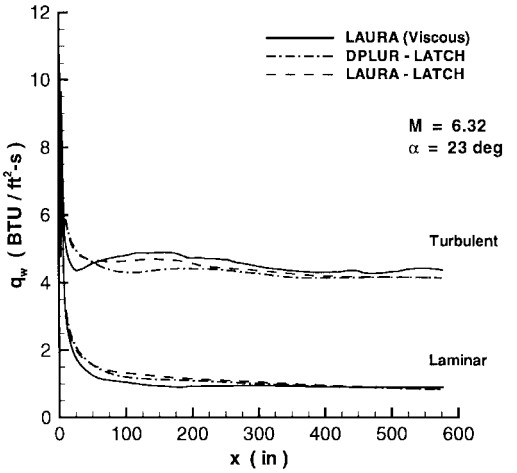

a) $t = 330$ s

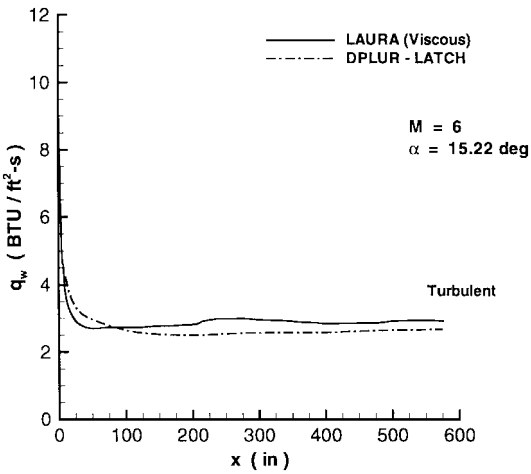

b) $t = 340$ s

Fig. 21 Windward centerline heating.

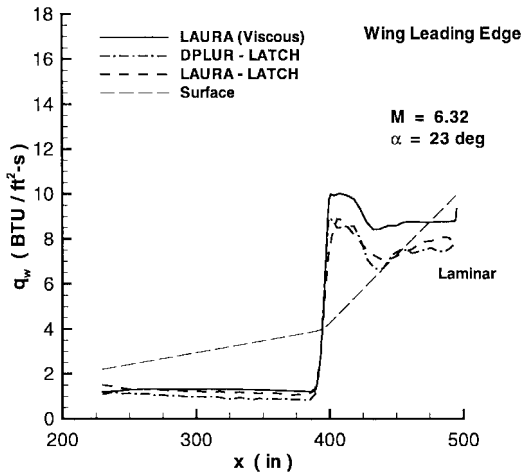

Fig. 22 Laminar wing leading edge heating at $t = 330$ s.

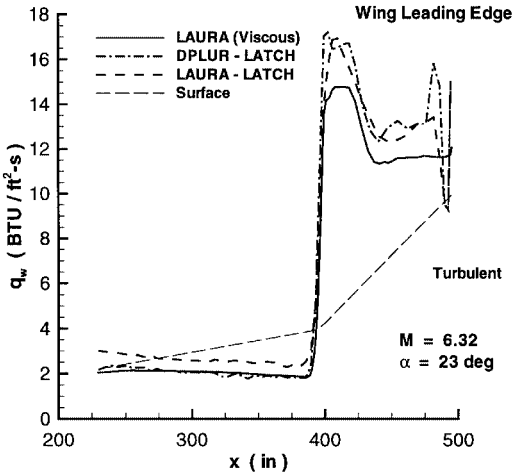

Fig. 23 Turbulent wing leading edge heating at $t = 330$ s.

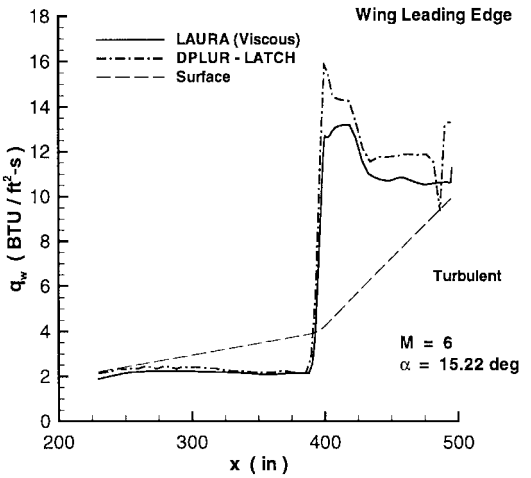

Fig. 24 Turbulent wing leading edge heating at $t = 340$ s.

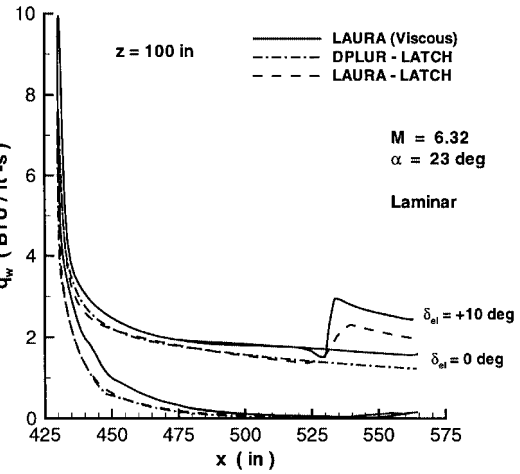

Fig. 25 Laminar wing heating at $t = 330$ s.

to peak temperatures (not shown) along the leading edge of 1800°F for LAURA and 1725°F for LATCH. As shown previously, it is the inviscid boundary-layer solutions that predict the higher turbulent heating rates as shown in Figs. 23 and 24. Turbulent peak temperatures are 2035°F ($t = 330$ s) and 1965°F ($t = 340$ s) from LAURA and 2110°F ($t = 330$ s) and 2020°F ($t = 340$ s) from LATCH. Silicone impregnated reusable ceramic ablator (SIRCA) tiles are used for the wing leading edge because these temperatures exceed the HHB limit of 2000°F. Overall, the inviscid boundary-layer method predicts reasonably good (within 15%) surface heating rates and radiative equilibrium surface temperatures along the wing leading edge, especially considering the strong bow/wing-shock interaction.

Wing heating distributions at $z = 100$ in. are presented in Figs. 25–27. Figures 25 and 26 show the effect of elevon deflection on the heating rates. The inviscid boundary-layer results agree well with the viscous LAURA solutions over much of the wing including the elevon. Heating rates from LATCH are approximately 20% lower than LAURA for the laminar case presented in Fig. 25 but are within 10% for the turbulent cases. Although not shown, the

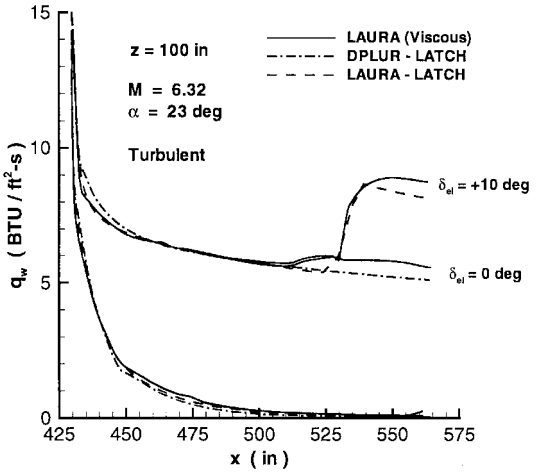

Fig. 26 Turbulent wing heating at t = 330 s.

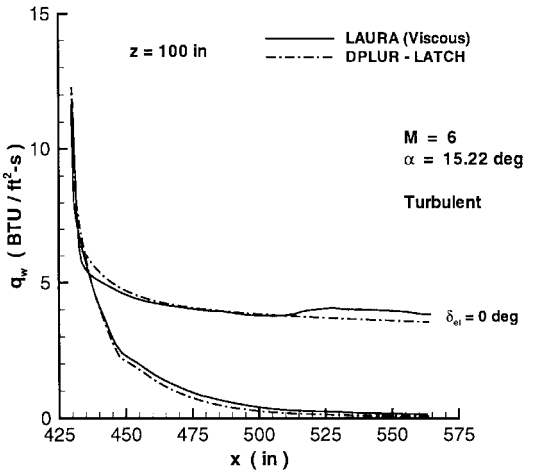

Fig. 27 Turbulent wing heating at t = 340 s.

deflected elevon results in increases of about 190°F for laminar flow and 240°F for turbulent flow over the surface temperatures of the undeflected elevon. Both LATCH and LAURA predict similar jumps in temperature.

Concluding Remarks

A combined inviscid boundary-layer method (LAURA–LATCH and DPLUR–LATCH) has been used to predict the surface heating rates and radiative equilibrium wall temperatures for the X-34 vehicle along a reference trajectory. This information has been delivered to OSC as part of a collective effort by NASA Langley Research Center to aid the TPS design. Wall-temperature patterns from the engineering boundary-layer code LATCH are similar to the wall temperatures from the N–S solver LAURA over much of the vehicle at two flight conditions. Increased temperatures along the wing because of the wing bow-shock interaction and on the deflected elevon are correctly predicted by the inviscid boundary-layer technique. LATCH predicts surface heating rates that are generally within 20% of values from a viscous LAURA solution. The observed agreement between LATCH and LAURA is somewhat better for turbulent flows. The turbulent radiative equilibrium surface temperatures are 300–600°F higher than the corresponding laminar temperatures at the same conditions. The inviscid boundary-layer method (DPLUR–LATCH and LAURA–LATCH) also uses much less computer time than the N–S solver LAURA. Consequently, many more solutions can be computed along a vehicle's trajectory with the same computational resources. This ability to generate a reasonably accurate aerothermal database for a vehicle makes inviscid boundary-layer methods excellent design tools.

References

[1]NASA, "Reusable Launch Vehicle (RLV), Small Reusable Booter, X-34," Cooperative Agreement Notice CAN 8-2, Jan. 1995.

[2]Smith, B. A., and Asker, J. R., "NASA Speeds Selection of X-33, X-34 Plans," *Aviation Week and Space Technology*, Vol. 142, No. 11, 1995, pp. 107–109.

[3]Asker, J. R., "X-34 to be Acid Test for Space Commerce," *Aviation Week and Space Technology*, Vol. 142, No. 14, 1995, pp. 44–53.

[4]Foley, T. M., "Big Hopes for Small Launchers," *Aerospace America*, Vol. 33, No. 7, 1995, pp. 28–34.

[5]Anselmo, J. C., "NASA Gives Second Shot at X-34," *Aviation Week and Space Technology*, Vol. 144, No. 25, 1996, p. 31.

[6]Eisele, A., "Orbital Sciences Gets X-34 Nod Again," *Space News*, Vol. 7, No. 25, 1996, p. 4.

[7]Freeman, D. C., Jr., Talay, T. A., and Austin, R. E., "Single-Stage-to-Orbit—Meeting the Challenge," *Acta Astronautica*, Vol. 38, No. 4–8, 1996, pp. 323–331.

[8]Engel, C. D., and Praharaj, S. C., "MINIVER Upgrade for the AVID System, Vol. I: LANMIN User's Manual," NASA CR-172212, Aug. 1983.

[9]Hamilton, H. H., II, Greene, F. A., and DeJarnette, F. R., "Approximate Method for Calculating Heating Rates on Three-Dimensional Vehicles," *Journal of Spacecraft and Rockets*, Vol. 31, No. 3, 1994, pp. 345–354.

[10]Thompson, R. A., "Comparison of Nonequilibrium Viscous-Shock-Layer Solutions with Shuttle Heating Measurements," *Journal of Thermophysics and Heat Transfer*, Vol. 4, No. 2, 1990, pp. 162–169.

[11]Lawrence, S. L., Chaussee, D. S., and Tannehill, J. C., "Application of an Upwind Algorithm to the Three-Dimensional Parabolized Navier–Stokes Equations," AIAA Paper 87-1112, June 1987.

[12]Wurster, K. E., Riley, C. J., and Zoby, E. V., "Engineering Aerothermal Analysis for X-34 Thermal Protection System Design," *Journal of Spacecraft and Rockets*, Vol. 36, No. 2, 1999, pp. 216–228.

[13]Kleb, W. L., Wood, W. A., Gnoffo, P. A., and Alter, S. J., "Computational Aeroheating Predictions for X-34," *Journal of Spacecraft and Rockets*, Vol. 36, No. 2, 1999, pp. 179–188.

[14]Berry, S. A., Horvath, T. J., DiFulvio, M., Glass, C., and Merski, N. R., "X-34 Experimental Aeroheating at Mach 6 and 10," *Journal of Spacecraft and Rockets*, Vol. 36, No. 2, 1999, pp. 171–178.

[15]Weilmuenster, K. J., and Gnoffo, P. A., "Solution Strategy for Three-Dimensional Configurations at Hypersonic Speeds," *Journal of Spacecraft and Rockets*, Vol. 30, No. 4, 1993, pp. 385–394.

[16]Alter, S. J., "Surface Modeling and Grid Generation of Orbital Sciences X34 Vehicle (Phase I)," NASA CR-97-206243, Nov. 1997.

[17]Gnoffo, P. A., "Code Calibration Program in Support of the Aeroassist Flight Experiment," *Journal of Spacecraft and Rockets*, Vol. 27, No. 2, 1990, pp. 131–142.

[18]Weilmuenster, K. J., and Greene, F. A., "HL-20 Computational Fluid Dynamics Analysis," *Journal of Spacecraft and Rockets*, Vol. 30, No. 5, 1993, pp. 558–566.

[19]Gnoffo, P. A., Weilmuenster, K. J., and Alter, S. J., "Multiblock Analysis for Shuttle Orbiter Re-Entry Heating from Mach 24 to Mach 12," *Journal of Spacecraft and Rockets*, Vol. 31, No. 3, 1994, pp. 367–377.

[20]Mitcheltree, R. A., and Gnoffo, P. A., "Wake Flow About the Mars Pathfinder Entry Vehicle," *Journal of Spacecraft and Rockets*, Vol. 32, No. 5, 1995, pp. 771–776.

[21]Weilmuenster, K. J., Gnoffo, P. A., Greene, F. A., Riley, C. J., Hamilton, H. H., II, and Alter, S. J., "Hypersonic Aerodynamic Characteristics of a Proposed Single-Stage-to-Orbit Vehicle," *Journal of Spacecraft and Rockets*, Vol. 33, No. 4, 1996, pp. 463–469.

[22]Gnoffo, P. A., Weilmuenster, K. J., Hamilton, H. H., II, Olynick, D. R., and Venkatapathy, E., "Computational Aerothermodynamic Design Issues for Hypersonic Vehicles," AIAA Paper 97-2473, June 1997.

[23]Roe, P. L., "Approximate Riemann Solvers, Parameter Vectors, and Difference Schemes," *Journal of Computational Physics*, Vol. 43, No. 2, 1981, pp. 357–372.

[24]Harten, A., "High Resolution Schemes for Hyperbolic Conservation Laws," *Journal of Computational Physics*, Vol. 49, No. 3, 1983, pp. 357–393.

[25]Yee, H. C., "On Symmetric and Upwind TVD Schemes," NASA TM-86842, Sept. 1985.

[26]Gnoffo, P. A., "Upwind-Biased, Point-Implicit Relaxation Strategies for Viscous, Hypersonic Flows," AIAA Paper 89-1972, June 1989.

[27]Cebici, T., "Behavior of Turbulent Flow near a Porous Wall with Pressure Gradient," *AIAA Journal*, Vol. 8, No. 12, 1970, pp. 2152–2156.

[28]Baldwin, B., and Lomax, H., "Thin-Layer Approximation and Algebraic Model for Separated Turbulent Flows," AIAA Paper 78-257, Jan. 1978.

[29]Cheatwood, F. M., and Gnoffo, P. A., "User's Manual for the Langley Aerothermodynamic Upwind Relaxation Algorithm (LAURA)," NASA TM-4674, April 1996.

[30]Gnoffo, P. A., "An Upwind-Biased, Point-Implicit Relaxation Algorithm for Viscous, Compressible Perfect-Gas Flows," NASA TP-2953, Feb. 1990.

[31]Candler, G. V., Wright, M. J., and McDonald, J. D., "Data-Parallel Lower-Upper Relaxation Method for Reacting Flows," *AIAA Journal*, Vol. 32, No. 12, 1994, pp. 2380–2386.

[32]Wright, M. J., Candler, G. V., and Prampolini, M., "Data-Parallel Lower-Upper Relaxation Method for the Navier–Stokes Equations," *AIAA Journal*, Vol. 34, No. 7, 1996, pp. 1371–1377.

[33]Yoon, S., and Jameson, A., "An LU-SSOR Scheme for the Euler and Navier–Stokes Equations," AIAA Paper 87-0600, Jan. 1987.

[34]Zoby, E. V., and Simmonds, A. L., "Engineering Flowfield Method with Angle-of-Attack Applications," *Journal of Spacecraft and Rockets*, Vol. 22, No. 4, 1985, pp. 398–405.

[35]Zoby, E. V., "Approximate Heating Analysis for the Windward Symmetry Plane of Shuttle-Like Bodies at Large Angle of Attack," *Thermophysics of Atmospheric Entry*, edited by T. E. Horton, Vol. 82, Progress in Astronautics and Aeronautics, AIAA, New York, 1982, pp. 229–247.

[36]Hamilton, H. H., II, DeJarnette, F. R., and Weilmuenster, K. J., "Application of Axisymmetric Analog for Calculating Heating in Three-Dimensional Flows," *Journal of Spacecraft and Rockets*, Vol. 24, No. 4, 1987, pp. 296–302.

T. C. Lin
Associate Editor